arXiv:2111.06322v3 [stat.AP] 2 Mar 2022

MONITORING A BOLTED VIBRATING STRUCTURE USING MULTIPLE ACOUSTIC EMISSION SENSORS: A BENCHMARK

Emmanuel Ramasso, Benoît Verdin, Gaël Chevallier
Department of Applied Mechanics
Institut FEMTO-ST, UBFC/UFC/ENSMM/CNRS/UTBM,
24 Rue Alain Savary, 25000 Besançon, France

ABSTRACT

The data set presented in this work, called ORION-AE, is made of raw AE data streams collected by three different AE sensors and a laser vibrometer during five campaigns of measurements by varying the tightening conditions of two bolted plates submitted to harmonic vibration tests. With seven different operating conditions, this data set was designed to challenge supervised and unsupervised machine/deep learning as well as signal processing methods which are developed for material characterization or Structural Health Monitoring (SHM). One motivation of this work was to create a common benchmark for comparing data-driven methods dedicated to AE data interpretation. The data set is made of time-series collected during an experiment designed to reproduce the loosening phenomenon observed in aeronautics, automotive or civil engineering structures where parts are assembled together by means of bolted joints. Monitoring loosening in jointed structures during operation remains challenging because contact and friction in bolted joints induce a nonlinear stochastic behavior. ORION-AE data set is available on the shared directory for Research Data, Harvard Dataverse at `https://doi.org/10.7910/DVN/FBRDU0`. A Matlab code is provided to extract the data stream from each sensor. This article is a preprint, the published version is available at `https://doi.org/10.3390/data7030031`.

Keywords Acoustic emission; Bolted joints; Health monitoring; Laser vibrometry; Benchmarking

1 Summary

Acoustic emission (AE) is one of the most promising non-destructive techniques for its ability to detect changes in the integrity of materials at the microscale. When a damage occurs, an elastic wave is released which propagates onto the surface creating displacements ranging from picometers to nanometers. The displacements are detected by highly sensitive piezoelectric sensors permanently attached onto a material. Data are continuously collected at sampling rate around 5 MHz. The obtained AE data stream (time-series) is then processed by algorithms to detect AE signals related to damages.

AE is used in many laboratories for materials characterization [21] and in industrial applications for real time monitoring of manufacturing process [23] or storage facilities [1]. Despite many publications on the topic, the precise identification of the source of AE signals remains a challenge. Indeed, AE source identification is an inverse problem which is difficult to solve due to the sensitivity of the sensors which provide many AE signals corrupted by noise, as well as due to the effects of wave propagation in damaged materials which creates wave scattering [20].

The lack of prior knowledge on AE sources compels AE users to interpret AE by means of unsupervised learning algorithms which include the following steps:

1. AE signals detection: Also called wave-picking (like in seismology [13]), this step aims at processing the AE data stream to keep only relevant signals, defined as being above a given threshold (minimum amplitude). A preprocessing step can be included using wavelet denoising in noisy cases [17, 11].

2. AE signals clustering: The signals obtained in the previous step fed a clustering method which aims at creating groups (clusters) of AE signals [31].
3. Clustering validation: The validation of the results obtained in the previous step is performed in a subjective manner because of the lack of prior knowledge of AE sources. To circumvent this problem, AE users apply different clustering strategies in the previous step and then compute clustering validity indices [26, 25] which provide a scalar value that allows end-users to compare different results. The results can also be visually analyzed, like in interactive clustering [4], to evaluate whether the clusters can be related to AE sources with a physical meaning [22].

An alternative to these three-steps strategy is based on anomaly detection [14, 15]. A baseline is considered to train a one-class supervised learning algorithm which can then be used to generate a health indicator for online monitoring [9]. Anomaly detection was also exploited for clustering in [18].

In real applications or for complex materials, AE signals detection (step 1), clustering (step 2) or validation (step 3), can be difficult. In that case, specific algorithms are developed. However, there is no common AE data sets that can serve as references (benchmark) to compare the methods of the literature. This work presents a benchmark data set that can be used for this purpose.

The experiment was designed to reproduce the loosening phenomenon observed in aeronautics, automotive or civil engineering structures where parts are assembled together by means of bolted joints. During the service life of a bolted structures, the torque can evolve according to operational conditions such as loading, in particular when these structures are submitted to vibrations. Monitoring the loosening condition in bolted structures during operation remains challenging because contact and friction in bolted joints induce a nonlinear stochastic behavior [7, 12, 16, 29, 3, 2]. A common solution consists in measuring the pretightening force using a strain gauge bonded on the top surface of a bolt head [28]. This is a local approach since we need to instrument every bolt. On the other hand, global techniques make use of only a few sensors for bolt condition monitoring. There are two categories of global techniques: active and passive approaches. Active approaches such as lamb waves were used in the past and consists in using a transmitter of high harmonics waveforms tuned to be sensitive to the changes in the contacts. The receiver is used to collect the waveforms after their propagation in the bolted structure. Machine learning can then be used to build an anomaly detector like in [9] and [15]. Conversely, passive approaches do not use an external source, but the transmitter is actually the structure itself (if a damage occurs). Therefore, a continuous reading of the piezoelectric sensors is necessary in order to not miss any damage or event. The use of AE sensors for condition monitoring of bolts is not frequent. For example, in recent works [30, 8], it was shown that high sensitivity piezoelectric sensors used in this technique are able to detect AE signals despite low signal-to-noise ratio in bolted joints under vibration.

In the context of stationary and harmonic vibration tests, the bolts can be subject to self-loosening under vibrations, eventually leading to a critical failure of the assembly. Therefore, it is of paramount importance to develop sensing strategies and algorithms for early loosening estimation. The main characteristics of this data set are the following:

- During the tests, the tightening level of one of the bolts was controlled to reach seven different values, from highly tightened to loosened. Therefore, the end-user knows that the tightening level has been set to a specific value for some periods of the data stream. This reference can be used either to train supervised (deep/transfer) learning methods (with possibly 7 classes) and for unsupervised or semi supervised learning. This reference can thus be helpful to validate steps 2 and 3 in the aforementioned methodology.
- The data set is made of raw acoustic emission data streams acquired by three different sensors and a laser vibrometer. Multisensor data fusion can thus be performed and evaluated using the reference. This can be helpful to improve algorithms in steps 2 and 3.
- The vibrometer data also allows use users to evaluate the performance of wave-picking algorithms with low signal-to-noise ratio. This can be helpful to validate step 1 in the aforementioned methodology.

2 Data Description

The data set was obtained on a test rig called ORION [8, 24]. It is constituted of a jointed structure, dynamically loaded with a vibration shaker and monitored with acoustic emission, force, and velocity sensors.

For each series of measurements, four sensors were used simultaneously: a laser vibrometer and three different AE sensors (micro80, F50A, micro200HF), each with a given frequency band, all sampled at 5 MHz, yielding approximately between 1.4 and 1.9 GB of data. A total of five series of measurements were performed denoted as *measurementSeries_B*, *measurementSeries_C*, *measurementSeries_D*, *measurementSeries_E* and *measurementSeries_F*.

The organization of repositories and files is depicted in Figure 1 for series of measurements B. There is one folder for each series of measurements. The ORION-AE data set is thus composed of five folders. For each series of measurements, there are seven subfolders corresponding to seven tightening levels: 60, 50, 40, 30, 20, 10, 05 cNm, except for *measurementSeries_C* for which 20 cNm is missing.

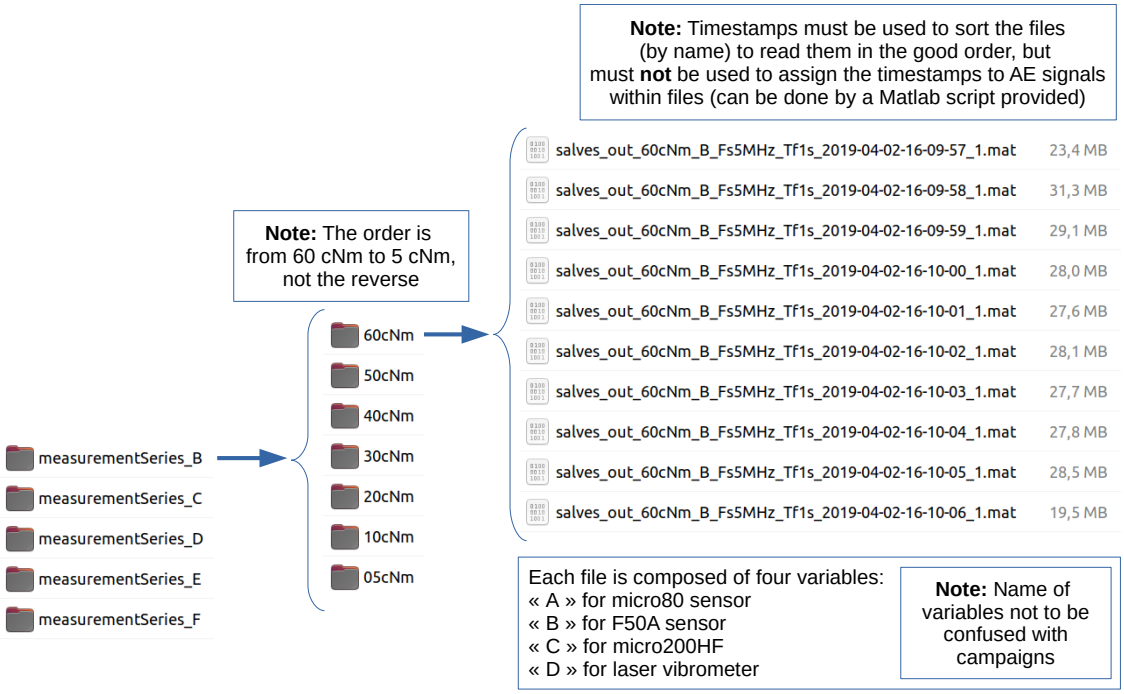


Figure 1: Tree structure of the repositories and files exemplified for series of measurements "B". The root directory on Dataverse also contains two additional repositories: One with images illustrating the content of the data in each level and campaign, and one with the sensors datasheet. Finally a Matlab script is provided to read the files and correctly extract the timestamps.

It is important to **read the subfolders in this precise order**, otherwise the physical meaning of the data becomes wrong. Th upper bolt have been untightened with a precise sequence. For example, reading from 5 cNm to 60 cNm (reverse order) does *not* correspond to the "tightening" of bolts since the process is not reversible in terms of acoustic emission characteristics.

Each subfolder is made of *.mat* files generated using MATLAB 2016b. There is about one file per second. The files in a subfolder are named according to the timestamps (time of recording) and must **be read in the correct order**. Each file has the following format:

salves_out_**X**cNm_**Y**_Fs5MHz_Tf1s_2019-04-02-**HH**-**MM**-**SS**_1.mat

where $\mathbf{X} \in \{5, 10, 20, 30, 40, 50, 60\}$ representing the tightening level, $\mathbf{Y} \in \{B, C, D, E, F\}$ for the series of measurements. The production date is "2019-04-02" and the timestamp began at HH-MM-SS. For example,

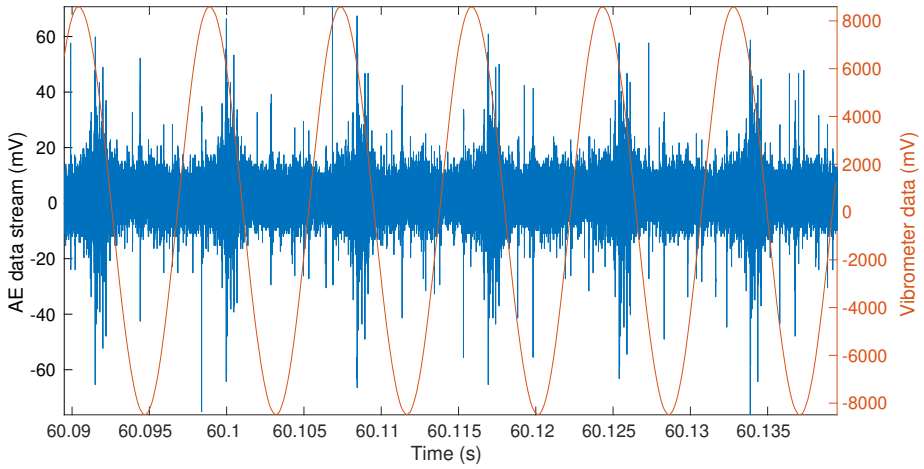
salves_out_05cNm_B_Fs5MHz_Tf1s_2019-04-02-16-22-09_1.mat

represents AE data for 5 cNm in series of measurements B taken at 16:22:09. Each *.mat* file is composed of vectors of data with the following names:

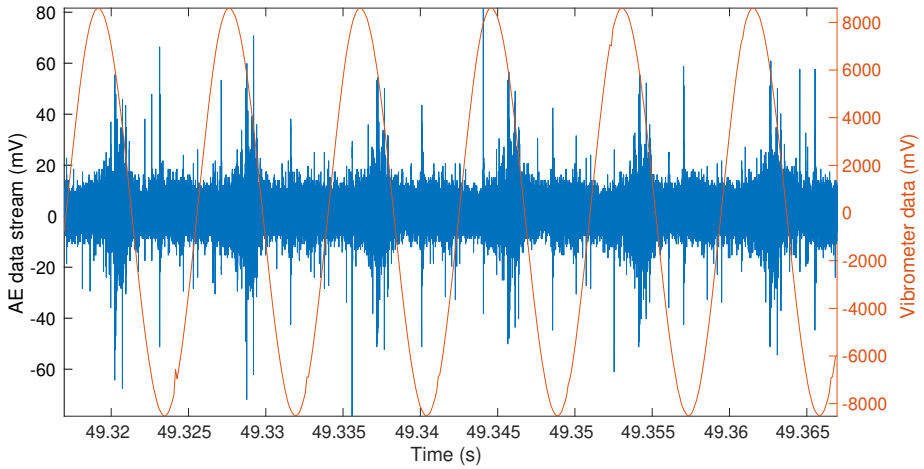
- Variable "A" corresponding to micro80 sensor data (sampling frequency: 5MHz).
- Variable "B" corresponding to F50A sensor data (sampling frequency: 5MHz).
- Variable "C" corresponding to micro200HF sensor data (sampling frequency: 5MHz).
- Variable "D" corresponding to laser velocimeter data (sampling frequency: 5MHz).

The number of samples is about 5×4 millions per file (each file corresponds to about 1 second), with all sensors data sampled at 5 MHz. The labels corresponding to the sensors must not be confused with the labels corresponding

to the test campaigns. Illustrations of the data are given in Figure 2 for sensor "F50A" (variable "B" in a file) in *measurementSeries_B*. About 6 periods are depicted (using the red curve representing the displacement of the upper beam).



(a) 5 cNm

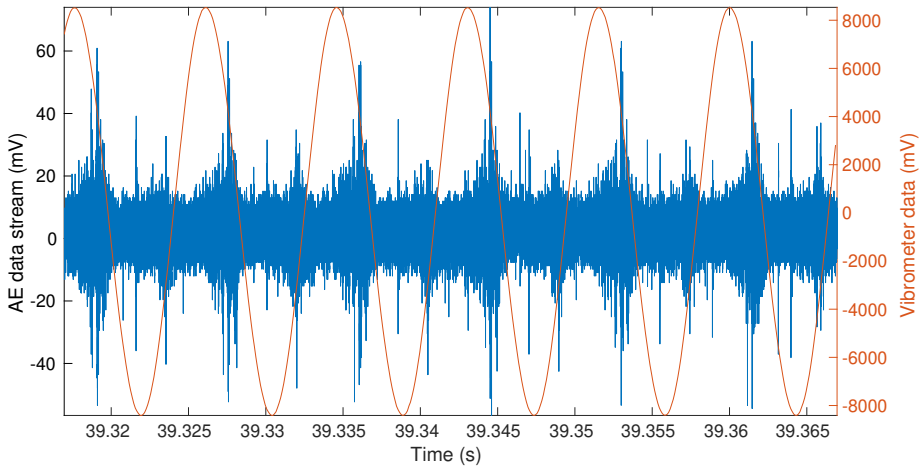


(b) 10 cNm

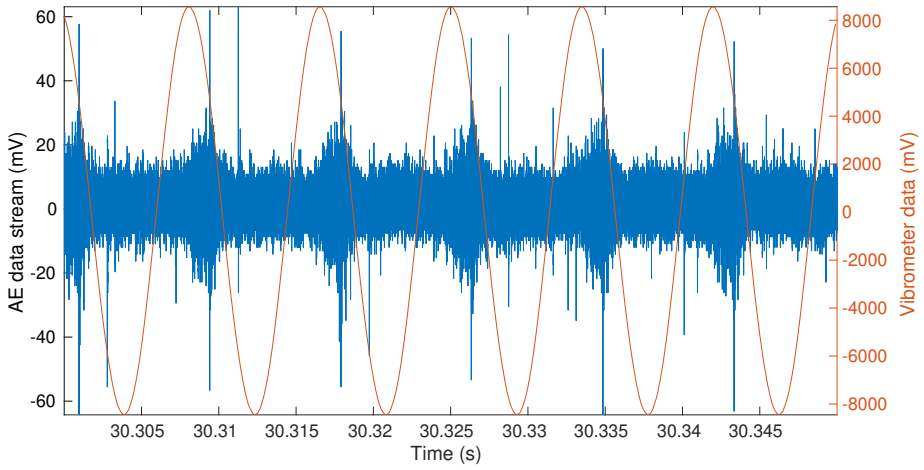
Figure 2: *Cont.*

Figure 3 depicts the acoustic emission and laser vibrometer data, superimposed with the labels (tightening levels) evolving from 1 to 7, for measurement B. This figure (red curve) shows that the **control of the displacement of the beam by a feedback from the laser vibrometer** (as explained in the "Method" Section) leads to a similar displacement during a whole test (about 70 s). In this figure, the green curve representing the acoustic emission shows that the amplitude can not be used as a feature to discriminate the levels.

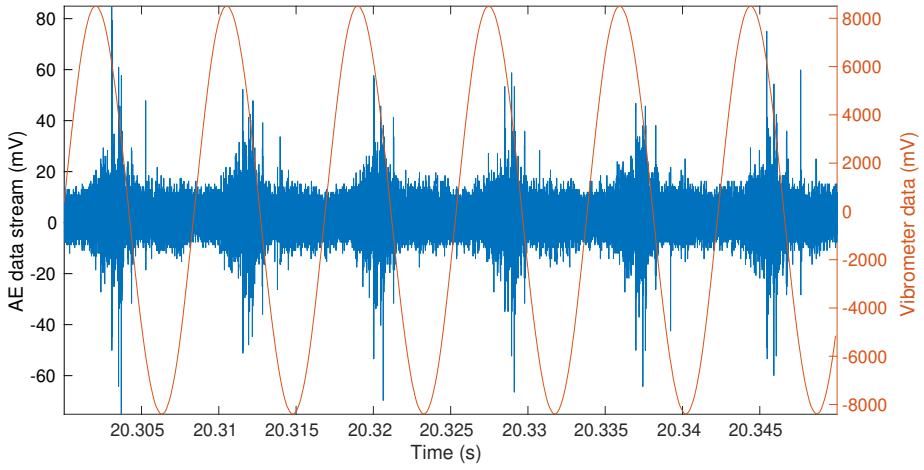
It is important to note that the real timestamps in filenames must not be taken as the timestamps of the AE signals in a data stream. The real timestamps must be calculated from the exact number of samples in each file, starting from $t = 0\,s$ for 60 cNm. There are about 10 s of continuous recording of data per level and for the four sensors. The exact duration of a period can be found according to the number of files in each subfolder, the number of points per file and the sampling frequency. The precise values are given in Table 1. A Matlab code (ORION_AE_sample_read_files.m) is provided in the data directory to read the files and reproduce the duration of each period.



(c) 20 cNm

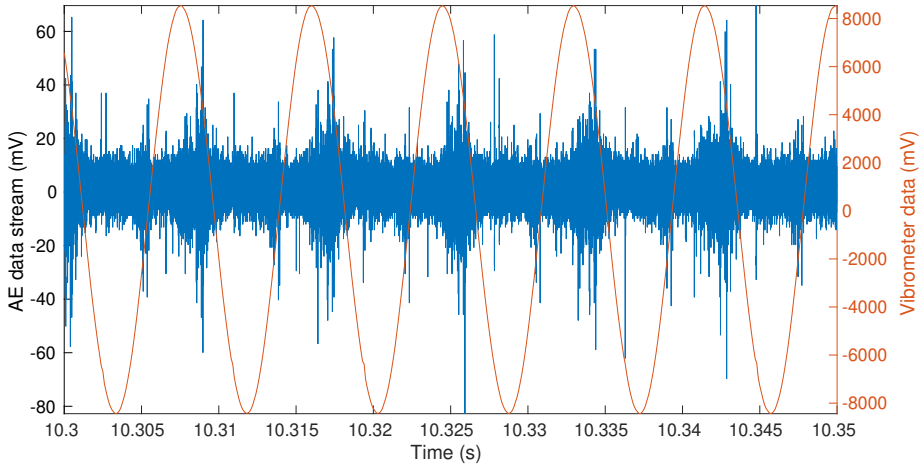


(d) 30 cNm

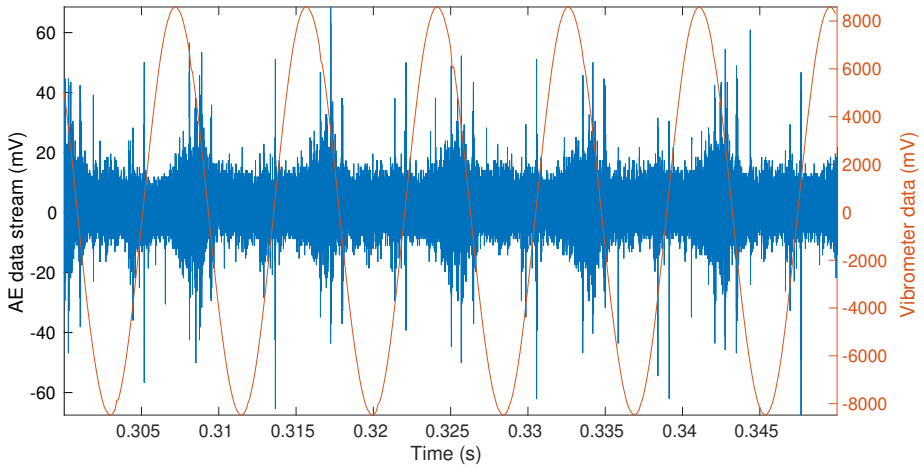


(e) 40 cNm

Figure 2: *Cont.*



(f) 50 cNm



(g) 60 cNm

Figure 2: (a–g) Sample of the data in measurement series "B" with sensor "F50A" for each tightening level. Blue curve: AE signal; red curve: laser vibrometer data (harmonic vibration signal at 100 Hz with amplitude control).

Meas. series	60 cNm	50 cNm	40 cNm	30 cNm	20 cNm	10 cNm	5 cNm
B	10.0000	10.0000	10.0000	9.0170	10.0000	10.7725	9.2275
C	10.0000	10.0000	10.0000	10.0000	N.A.	10.0000	10.0000
D	10.0000	10.0000	10.8119	9.1881	10.0000	10.0000	10.0000
E	10.0000	10.0000	10.0000	10.0000	10.0000	10.0000	10.0000
F	10.0000	10.0000	10.0000	10.0000	10.0000	10.0000	10.0000

Table 1: Duration in seconds of each period for a given tightening level. The exact duration of a period can be found according to the number of files in each subfolder, the number of points per file and the sampling frequency. This table can be reproduced using a A Matlab code (ORION_AE_sample_read_files.m) provided in the data directory.

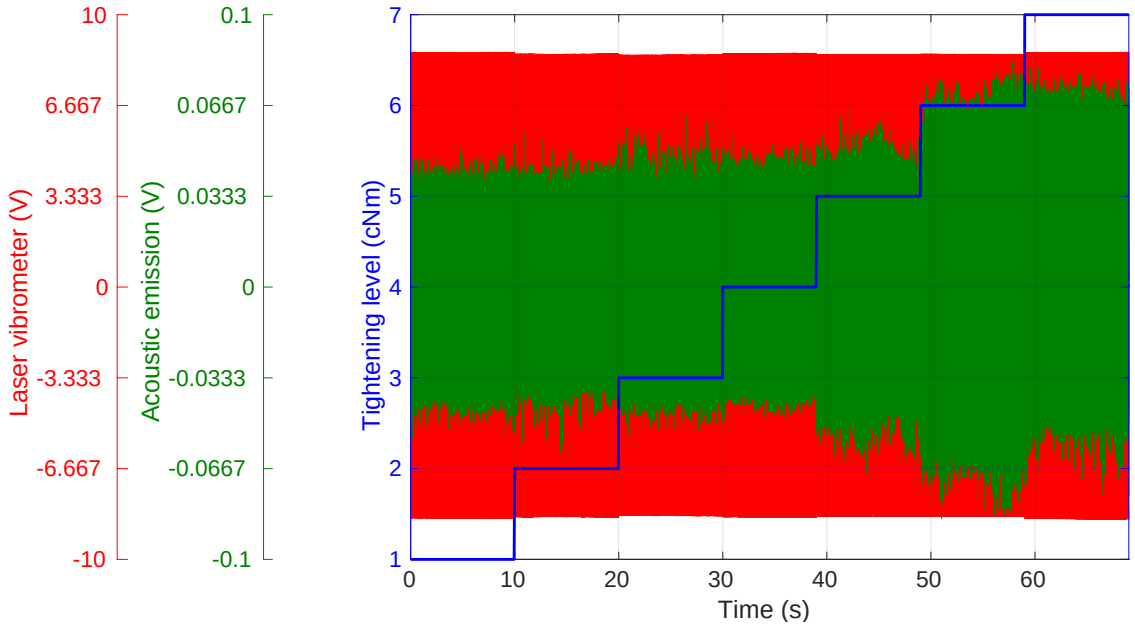


Figure 3: Tightening levels, acoustic emission and laser vibrometer data superimposed for measurements "B" and sensor micro-200-HF (variable C). Due to the amount of data involved, a subsampling by a factor of 10 was applied for each file. The x-axis is here represented using the time of test (about 70 s), starting from 60 cNm from the left (around between $t \in [0, 10]$ s) to 5 cNm on the right (from $t > 60$ s).

3 Methods

The ORION test rig (Figure 4) has been designed for the study of vibration damping and makes the vibration tests highly reproducible as shown in [8, 24]. It is a jointed structure made of two plates manufactured with 2024 aluminium alloy, linked together by three M4 bolts (Figure 4). Contact patches are machined overlays which have been added at each bolt connection to retain the contact between both beams in a small area, minimizing uncertainties on the structure's response and enhancing the repeatability between measurements. The contact patches have an area of 12×12 mm^2 and are 2 mm thick. The central bolt is dedicated to "static" functions, i.e. to ensure structural integrity and provide resistance to dynamic loads without substantial stiffness changes. The external bolts, in turn, perform "damping" functions, i.e. to increase energy dissipation due to frictional contact. It is worth noticing that these two functions have to be monitored in order to ensure the integrity (central bolt) and the damping (lateral bolts).

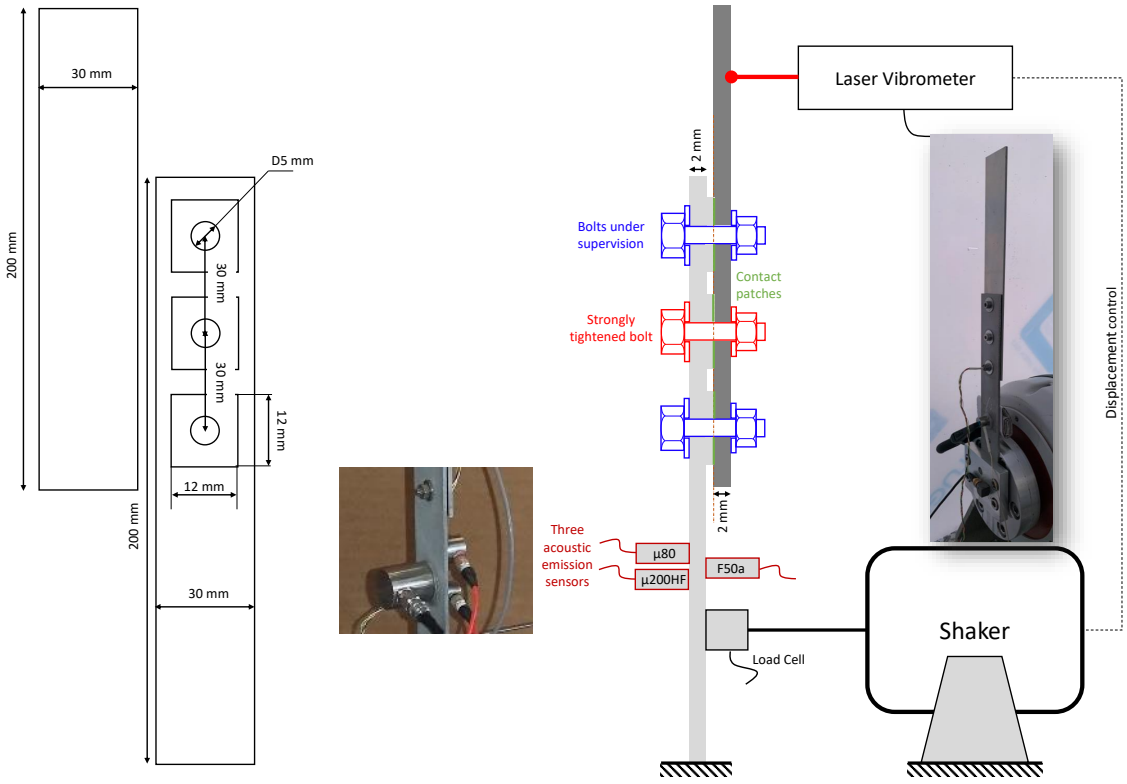


Figure 4: Setup description: part dimensions, sensors positions, bolts positions

The harmonic excitation load was applied using a Tira TV51120, electromagnetic shaker which can deliver a $200N$ force. The structure was submitted to a 100 Hz harmonic excitation force during about 10 s. The force was measured using a PCB 208C02 piezoelectric force sensor.

The vibration magnitude was measured using a Polytec PSV500Xtra, laser vibrometer. The obtained laser data allowed us to make sure that the amplitude of the displacement of the top of the upper plate remains constant for all tightening levels.

Seven tightening levels, corresponding to seven operating conditions of the structure under vibration, were applied on the upper bolt. The tightening level was first set to 60 cNm with a torque screwdriver. After about a 10 s vibration test, the shaker was stopped and this vibration test was repeated after a torque modification at 50 cNm. Then torque modifications at 40, 30, 20, 10 and 5 cNm were applied. The change in the tightening level was made using a CDI torque screwdrivers. The torque was checked three times at each change.

The acoustic emission sensors used were a "micro-200-HF", a "micro-80" and a "F50A", made by Euro-Physical Acoustics. They were connected to a preamplifer set to 60 dB (model 2/4/6 preamplifier made by Europhysical acoustics). Their detailed characteristics, such as dimensions and frequency bands, are provided in the datasheets enclosed in the data set, with a summary of the main ones given in Table 2. The sensors were attached onto the lower plate (5 cm above the end of the plate) using a silicone grease. All data were sampled at 5 MHz using a Picoscope

4824 (20 MHz bandwidth, low noise, 12-bit resolution, 256 MS buffer memory, USB 3) connected to a linux PC with MATLAB® 2016b and the Data Acquisition® toolbox. The datasheet of the Picoscope is provided in the data set.

	Units	F50A	micro80	micro200HF
Peak Sensitivity, Ref V/(m/s)	dB	65	57	62
Operating Frequency Range (kHz)	kHz	200-800 kHz	200-900	500-4500
Resonant Frequency, Ref V/(m/s)	kHz	100 kHz	250	2500

Table 2: Frequency and sensitivity of the acoustic emission sensors used. The data sheets are provided in the data set.

4 User notes

4.1 About the ground truth

In ORION-AE data set, we know that, during each period of 10 s, the tightening level has been set to a specific value. The tightening level can be considered as constant during each period, and therefore can be used as a reference. However, during each cycle of the vibration test for a given tightening level, different AE sources can generate AE signals and those sources may be activated or not, depending on the tribological conditions which are not known. The tightening level may thus slightly change during the period of 10 seconds. The tribological conditions may also be different from a campaign to another. Despite this variability, preliminary results shown in [19] demonstrated that the content of AE signals in those series of measurements is sufficient to discriminate between the periods, which seem to corroborate that, first, the AE sources have indeed a signature depending on the tightening level, and second, that the tightening level and the amplitude of the vibrations (controlled by a closed-loop using the laser vibrometer) remains constant during the period of $10\,s$.

4.2 ORION-AE for AE signal detection

In addition to machine learning tasks, this data set can be used for signal processing and in particular *wave-picking* (step 1, presented in introduction). As for seismic wave detection [5], this step aims at finding relevant signals in a data stream. Wave-picking is one the most important task in acoustic emission analysis because it paves the way for feature extraction, classification, localization of acoustic emission sources and interpretation by machine learning.

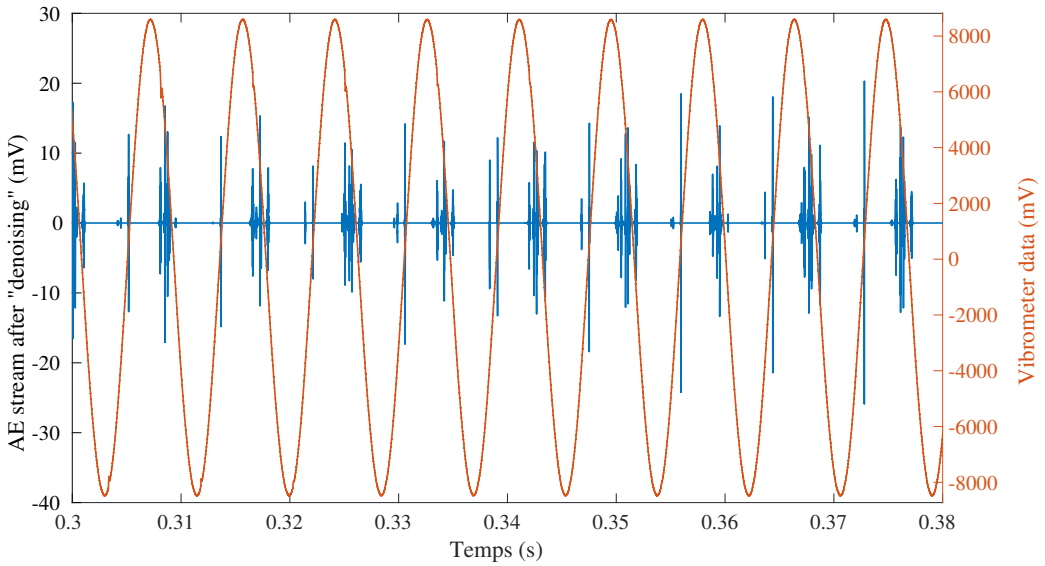
In ORION-AE, the AE sources are related to tribological phenomenon characterized by low amplitude and with low signal-to-noise ratio. Denoising methods are thus generally used as a preprocessing step. Figure 5 depicts the result of wavelet denoising with 14 levels of decomposition and using a Daubechies "db45" wavelet (the same settings as [11]). This was done for two sensors in the same chunk of data as shown in Fig. 5(a) and 5(b). It can be observed that the responses of the sensors differ since they have different characteristics (in particular the sensitivity and frequency band). We can also observe the presence of AE signals that occur at each cycle with some regularity.

We took the starting time, called onsets, of each signal detected after wavelet denoising (from Figure 5 using [11]). Onsets were then reported onto the vibrometer data in Figure 6. Each blue circle corresponds to one AE signal detected. The vertical position represents the amplitude of the displacement (measured by the vibrometer) when the signal was detected. We can observe that the amplitude is very similar between cycles (there is about 1 second of test represented on this figure), which means that the activation of the AE sources is highly reproducible between cycles. Similar results have been observed on other levels and considering measurements B to F. However, we also observed that several AE sources can occur in some levels, and that the average amplitude of displacement can change. It means that the instant of activation of the AE sources (related to the signals) seems to depend on the tightening levels. These observations can be dependent on the wave-picking algorithm used (here [11]) and should be confirmed in the future.

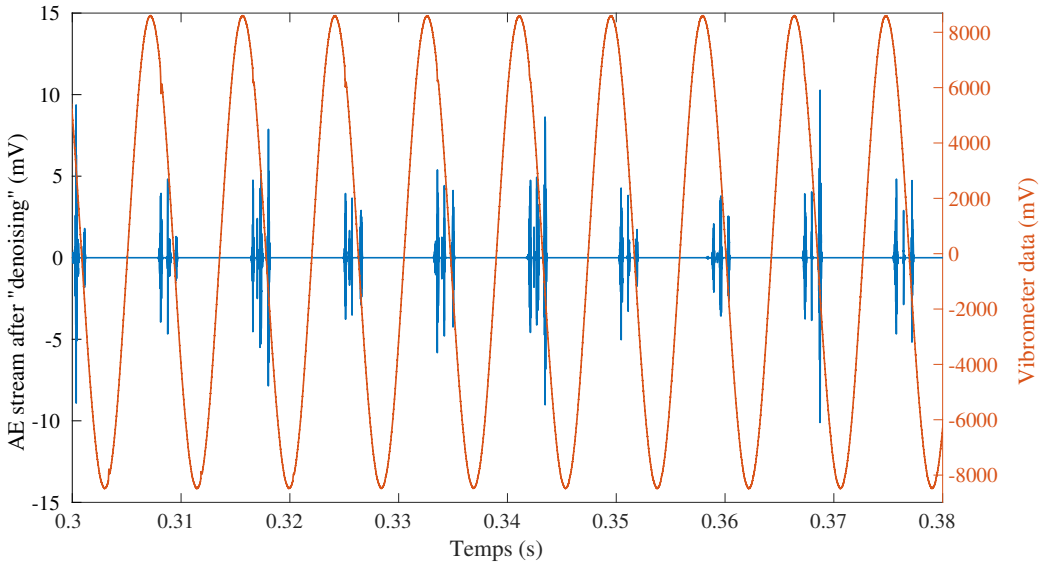
4.3 Possible challenges

ORION-AE data set can be used for different tasks.

Train supervised learning methods The classification task can consider up to 7 classes in order to discriminate between the levels using various machine and deep learning methods such as support vector machines or neural networks [6, 10]. By considering only the tightened levels, such as 60 cNm and 50 cNm, it can also be used to evaluate anomaly detectors based on autoencoders, self-organizing maps or one-class classifiers [9, 15]. In both cases, it is possible to use convolutionnal neural networks (CNN) taking as inputs the RGB images computed by the continuous wavelet transform (CWT) of the raw signals in each cycle. Cycles can be



(a) After wavelet denoising: Measurement B, first file in 60 cNm, sensor "F50A" (sensor 2).



(b) After wavelet denoising: Measurement B, first file in 60 cNm, sensor "micro-200-HF" (sensor 3).

Figure 5: Presence of signals in each cycle after wavelet denoising using two sensors (on the same period of time). For a given tightening level, the displacement measured by the vibrometer is quite close for each signal found at different cycles showing the reproducibility of the test rig.

precisely obtained by using a zero-crossing detector on the vibrometer data. Illustration of such CWT images are depicted in Figure 7 using two measurements series (B, D).

Data normalization aims at compensating time-varying operational variations which can occur in a system. According to our experience on this data set, it seems that, for a given tightening level, the signature of the signals accross campaigns seems to change. This can be due to the tribological conditions in the contacts that change between levels and campaigns. The classification algorithms (using deep learning and autoencoders) that we tested seem to work well when we mix levels and campaigns. However, the classification performance drastically drops when we distinguish the campaigns (for example training on B, C, D, E and testing on F supposed unknown as in a SHM task). A data normalization is thus needed (starting from data in the first levels, for example 60 cNm or $\{60, 50\}$ cNm). This is an important topic in SHM as presented in [9, Chap. 12].

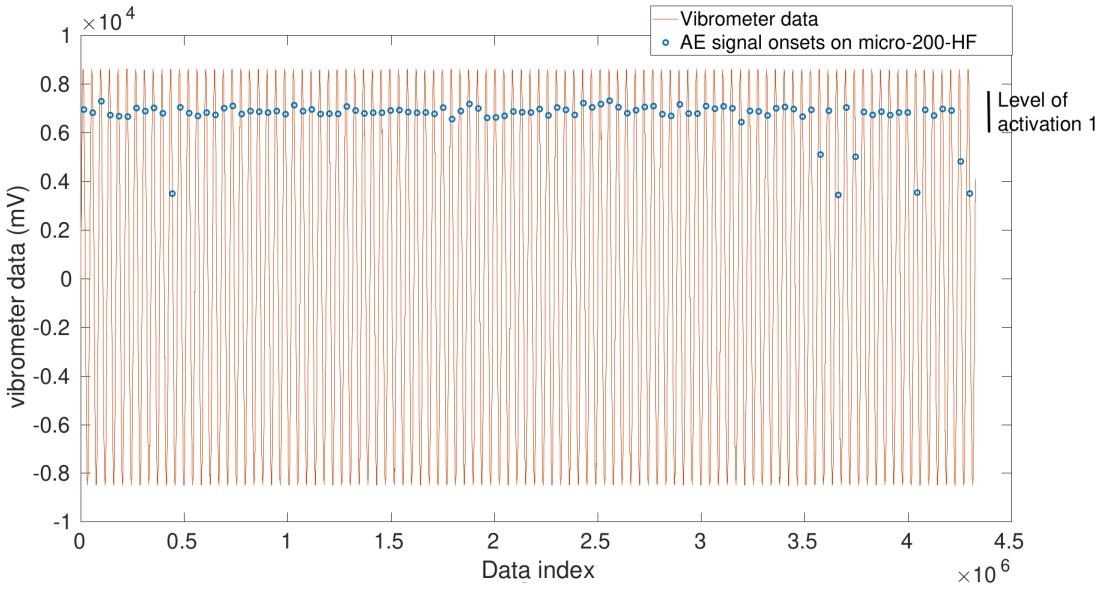


Figure 6: Acoustic emission onsets found by [11] and positioned onto vibrometer data for measurement B, first file in 60 cNm, sensor "micro-200-HF". The vertical position of the blue circle corresponds to the amount of displacement required to activate the AE sources. A similar amount is found in each cycle which illustrate the reproducibility of the test rig.

Validate unsupervised learning (clustering) using the tightening levels as a reference to be compared with, using, for example, the Adjusted Rand Index [27]. Initial results on this data set can be found in [19] using various algorithms.

Challenge wave-picking algorithms by trying to find either one set of signals per cycle or a set of several signals per cycle which should occur at similar displacement level along cycles for a given tightening level. Some results have been presented in the previous paragraphs using the method [11].

The generalization capabilities of the methods can be evaluated by considering different campaigns for training and testing. This is a critical point for structural health monitoring tasks.

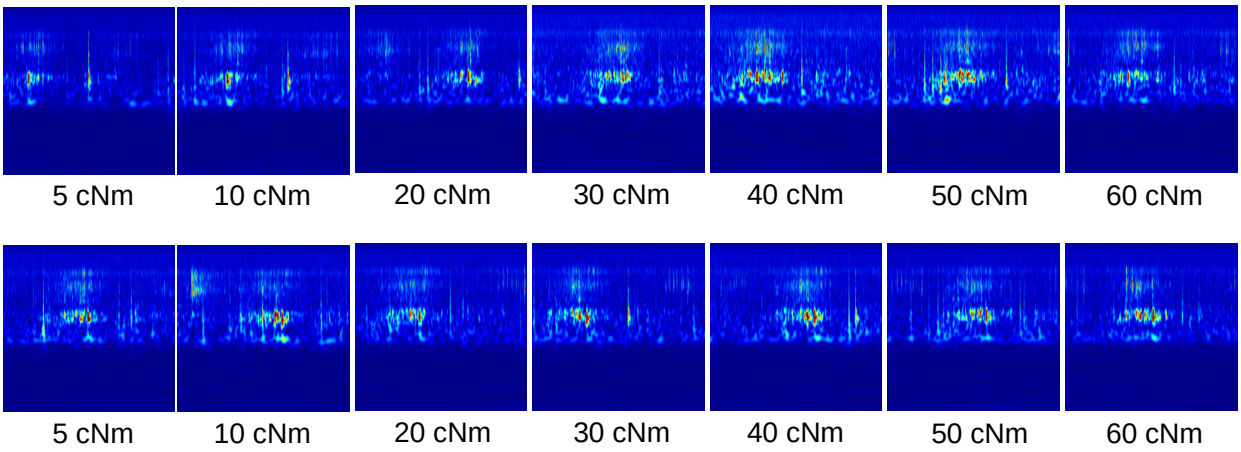


Figure 7: Continuous wavelet transform (CWT) images extracted for some cycles in sensor "F50A" (vector B) in measurement B (top figures) and in measurement D (bottom figures). Extraction of cycles can be automatically made by detecting zero-crossing in the vibrometer data (vector D).

4.4 Potential sources of error or variability

According to our experience on this data set, the low signal-to-noise ratio represents a real challenge to solve the three aforementioned tasks. Some preliminary results have been shown in [19] with a good performance of various clustering methods. These results were obtained by considering campaigns independently. Therefore, this study shown that the information hold by the data are relevant for estimating the tightening levels.

The variability accross campaigns can represent a difficulty for simple classification methods, as discussed in the previous section. To tackle this issue, a proper data normalization is needed.

In terms of error in the data set, we are aware that one level is missing: 20 cNm in campaign C. It means that this campaign is made of six classes.

This data set was already used by Master students in 2021 and 2022 for machine learning illustration and a SHM course, at both the University of Franche-Comté and National Engineering School of Mechanics and Microtechnics of Besançon, who reported only one issue concerning the presence of a directory "5cNm" (made of one file) in addition to "05cNm" (made of 9 files). This folder appears after the downloading but not on the online directory. We recommend to delete the former after having transfered the file in the latter. This "phantom" directory is a small issue reported to the support of Harvard Dataverse and still under consideration at the time of writing the present work.

Finally, we acknowledge that this data set is not representative of all possible data sets that can be collected using the AE technique. The purpose of this data set is simply to provide a common reference to researchers in the AE community interested in developing new machine / deep learning or pattern recognition methods or new algorithms dedicated for AE data interpretation. With the expansion of deep learning, we think that this data set can be useful for benchmarking, which can give a hand in discovering new and better ways of processing and interpreting acoustic emission data.

5 Data availability

Directory name: Harvard Dataverse.

Data identification number: 10.7910/DVN/FBRDU0.

Direct URL to data: `https://doi.org/10.7910/DVN/FBRDU0`, comprising a Matlab code to read the files. Codes and main results will be updated on `https://github.com/emmanuelramasso/ORION_AE_acoustic_emission_multisensor_datasets_bolts_loosening`.

Acknowledgement

This work was partly carried out in the framework of: EIPHI Graduate school (contract ANR-17-EURE-0002), project RESEM-COALESCENCE funded by "Institut de Recherche Technologique" Matériaux Métallurgie Procédés (IRT M2P) and "Agence Nationale de la Recherche" (ANR); project CLIMA funded by the "Fond Unique Interministériel" (FUI 19). The authors are also thankful to MIFHySTO and AMETISTE platforms.

References

[1] Li Ai, Vafa Soltangharaei, Mahmoud Bayat, Bruce Greer, and Paul Ziehl. Source localization on large-scale canisters for used nuclear fuel storage using optimal number of acoustic emission sensors. *Nuclear Engineering and Design*, 375:111097, 2021.

[2] Francesco Amerini and Michael Meo. Structural health monitoring of bolted joints using linear and nonlinear acoustic/ultrasound methods. *Structural health monitoring*, 10(6):659–672, 2011.

[3] Kassahun Asamene and Mannur Sundaresan. Analysis of experimentally generated friction related acoustic emission signals. *Wear*, 296(1-2):607–618, 2012.

[4] Juhee Bae, Tove Helldin, Maria Riveiro, Sławomir Nowaczyk, Mohamed-Rafik Bouguelia, and Göran Falkman. Interactive clustering: a comprehensive review. *ACM Computing Surveys (CSUR)*, 53(1):1–39, 2020.

[5] Christian Baillard, Wayne C Crawford, Valérie Ballu, Clément Hibert, and Anne Mangeney. An automatic kurtosis-based p-and s-phase picker designed for local seismic networks. *Bulletin of the Seismological Society of America*, 104(1):394–409, 2014.

[6] C.M. Bishop. *Pattern Recognition and Machine Learning*. Springer, 2006.

[7] Yixuan Chen, Jian Jiang, Xiaojun Qin, and Qian Feng. Quantitative monitoring of bolt looseness using multichannel piezoelectric active sensing and cbam-based convolutional neural network. *Advanced Sensing, Materials and Intelligent Algorithms for Multi-Domain Structural Health Monitoring*, page 710404126, 2022.

[8] G. Chevallier, E. Ramasso, and P. Butaud. Detection and analysis of loosening in jointed structures using acoustic emission sensors and smart bolts. In *37th Int. Conference on Modal Analysis*, pages 1–3, Florida, USA, 2019.

[9] C.R. Farrar and K. Worden. *Structural Health Monitoring: A Machine Learning Perspective*. John Wiley & Sons, Ltd, 2013.

[10] Daniel Frank Hesser, Shimaalsadat Mostafavi, Georg Karl Kocur, and Bernd Markert. Identification of acoustic emission sources for structural health monitoring applications based on convolutional neural networks and deep transfer learning. *Neurocomputing*, 453:1–12, 2021.

[11] M. Kharrat, E. Ramasso, V. Placet, and M.L. Boubakar. A signal processing approach for enhanced acoustic emission data analysis in high activity systems: Application to organic matrix composites. *Mechanical Systems and Signal Processing*, 70:1038–1055, 2016.

[12] Ning Li, Furui Wang, and Gangbing Song. Monitoring of bolt looseness using piezoelectric transducers: Three-dimensional numerical modeling with experimental verification. *Journal of Intelligent Material Systems and Structures*, 31(6):911–918, 2020.

[13] Zefeng Li, Men-Andrin Meier, Egill Hauksson, Zhongwen Zhan, and Jennifer Andrews. Machine learning seismic wave discrimination: Application to earthquake early warning. *Geophysical Research Letters*, 45(10):4773–4779, 2018.

[14] Sergio Martin-del Campo and Fredrik Sandin. Online feature learning for condition monitoring of rotating machinery. *Engineering Applications of Artificial Intelligence*, 64:187–196, 2017.

[15] Vahid Nasir and Farrokh Sassani. A review on deep learning in machining and tool monitoring: methods, opportunities, and challenges. *The International Journal of Advanced Manufacturing Technology*, 115(9):2683–2709, 2021.

[16] Seyed Majid Yadavar Nikravesh and Masoud Goudarzi. A review paper on looseness detection methods in bolted structures. *Latin American Journal of Solids and Structures*, 14:2153–2176, 2017.

[17] E. Pomponi, A. Vinogradov, and A. Danyuk. Wavelet based approach to signal activity detection and phase picking: Application to acoustic emission. *Signal Processing*, 115:110 – 119, 2015.

[18] Emmanuel Ramasso, Pauline Butaud, Thomas Jeannin, Fabrizio Sarasini, Vincent Placet, Nathalie Godin, Jacopo Tirillò, and Xavier Gabrion. Learning the representation of raw acoustic emission signals by direct generative modelling and its use in chronology-based clusters identification. *Engineering Applications of Artificial Intelligence*, 90:103478, 2020.

[19] Emmanuel Ramasso, Thierry Denoeux, and Gael Chevallier. Clustering acoustic emission data streams with sequentially appearing clusters using mixture models, 2021.

[20] F. Schubert and B. Schechinger. Numerical modeling of acoustic emission sources and wave propagation in concrete. In *NDTnet*, volume 7, pages 1–6, 2002.

[21] Aleksander Sendrowicz, Aleksander Omholt Myhre, Seweryn Witold Wierdak, and Alexei Vinogradov. Challenges and accomplishments in mechanical testing instrumented by in situ techniques: Infrared thermography, digital image correlation, and acoustic emission. *Applied Sciences*, 11(15), 2021.

[22] Aleksander Sendrowicz, Aleksander Omholt Myhre, Seweryn Witold Wierdak, and Alexei Vinogradov. Challenges and accomplishments in mechanical testing instrumented by in situ techniques: Infrared thermography, digital image correlation, and acoustic emission. *Applied Sciences*, 11(15):6718, 2021.

[23] Sergey A Shevchik, Giulio Masinelli, Christoph Kenel, Christian Leinenbach, and Kilian Wasmer. Deep learning for in situ and real-time quality monitoring in additive manufacturing using acoustic emission. *IEEE Transactions on Industrial Informatics*, 15(9):5194–5203, 2019.

[24] Rafael de O Teloli, Pauline Butaud, Gaël Chevallier, and Samuel da Silva. Good practices for designing and experimental testing of dynamically excited jointed structures: The orion beam. *Mechanical Systems and Signal Processing*, 163:108172, 2022.

[25] L. Vendramin, R.J.C.B. Campello, and E.R Hruschka. Relative clustering validity criteria: A comparative overview. *Statistical Analysis and Data Mining*, 3(4):209–235, 2010.

[26] Lucas Vendramin, Pablo A Jaskowiak, and Ricardo JGB Campello. On the combination of relative clustering validity criteria. In *Proceedings of the 25th Int. Conf. on Scientific and Statistical Database Management*, page 4. ACM, 2013.

[27] N.X. Vinh, J. Epps, and J. Bailey. Information theoretic measures for clusterings comparison: Is a correction for chance necessary? In *Proc. of the 26th Annual Int. Conference on Machine Learning*, pages 1073–1080, New York, NY, USA, 2009. ACM.

[28] Tao Wang, Bohai Tan, Guangtao Lu, Ben Liu, and Dan Yang. Bolt pretightening force measurement based on strain distribution of bolt head surface. *Journal of Aerospace Engineering*, 33(4):04020034, 2020.

[29] Z Zhang, Y Xiao, YQ Liu, and ZQ Su. A quantitative investigation on vibration durability of viscoelastic relaxation in bolted composite joints. *Journal of Composite Materials*, 50(29):4041–4056, 2016.

[30] Zhen Zhang, Yi Xiao, Zhongqing Su, and Yongdong Pan. Continuous monitoring of tightening condition of single-lap bolted composite joints using intrinsic mode functions of acoustic emission signals: a proof-of-concept study. *Structural Health Monitoring*, 18(4):1219–1234, 2019.

[31] Wei Zhou, Wen-zheng Zhao, Yan-nan Zhang, and Zhen-jun Ding. Cluster analysis of acoustic emission signals and deformation measurement for delaminated glass fiber epoxy composites. *Composite Structures*, 195:349–358, 2018.